Curvature-based approach to determining the optimal temperature regulation ranges for greenhouse peppers across growth stages

Jinghua Xu[1,2], Minke Hong[1,2], Miao Lu[1,2], Xudong Hu[1,2], Pan Gao[2,3], Jin Hu[2,3,4*], Qingxue Li[5*]

(1. *College of Mechanical and Electronic Engineering, Northwest A & F University, Yangling 712000, Shaanxi, China*;
2. *Key Laboratory of Agricultural Internet of Things, Ministry of Agriculture and Rural Affairs, Yangling 712000, Shaanxi, China*;
3. *College of Information Engineering, Northwest A & F University, Yangling 712000, Shaanxi, China*;
4. *Shaanxi Engineering Research Center of Agricultural Information Intelligent Perception and Analysis, Yangling 712000, Shaanxi, China*;
5. *Information Technology Research Center, Beijing Academy of Agriculture and Forestry Sciences, Beijing 100097, China*)

Abstract: In protected agriculture, extreme temperatures can cause irreversible damage to crops, making temperature regulation a critical component of greenhouse environmental management. The dynamic optimization of the temperature ranges serves as the core strategy to enhance production stability. Consequently, identifying the optimal temperature ranges is pivotal for maximizing greenhouse production efficiency. This study proposes a novel method for determining the optimal regulation ranges throughout the multiple growth stages of greenhouse-grown peppers, incorporating curvature theory. A nested experiment was designed to obtain the photosynthetic rate (Pn) of peppers during the multiple growth stages under variable temperature, CO_2 concentration, and photosynthetic photon flux density. A photosynthetic rate prediction model was then constructed using a backpropagation neural network optimized by a genetic algorithm, with an R^2 of 0.9812 and an MSE of 1.35 μmol/(m²·s). The prediction model was subsequently discretized and applied to calculate the Gaussian response surface of Pn. Finally, the U-chord algorithm and the random restart hill-climbing method were employed to precisely define the boundaries of the temperature regulation ranges. Practice demonstrated that the average dry weight of pepper fruits in the experimental group was 96.83% higher than that of the no-operation regulation group and 243.65% higher than the fixed threshold group. This method not only enhances pepper growth but also exhibits superior regulatory tolerance. Its innovative temperature regulation strategy provides crucial technical support and establishes a reliable decision-making basis for the precise environmental management of greenhouse crops in protected agriculture.

Keywords: photosynthetic rate prediction model, curvature theory, target boundary, greenhouse temperature regulation, machine learning
DOI: 10.25165/j.ijabe.20261902.10170

Citation: Xu J H, Hong M K, Lu M, Hu X D, Gao P, Hu J, et al. Curvature-based approach to determining the optimal temperature regulation ranges for greenhouse peppers across growth stages. Int J Agric & Biol Eng, 2026; 19(2): 65–77.

1 Introduction

In protected production, extreme temperatures in greenhouses can cause damage to crops in the form of blossom and fruit drop, stunting, and other injuries[1,2]. Traditional greenhouse temperature regulation has predominantly relied on the fixed threshold method[3,4] or the pursuit of maximum photosynthetic rate (Pn) to ensure optimal production[5]. However, the former imposes strict limitations through thresholds, leading to delayed responses and a disconnect from the physiological requirements of crops. While the latter can temporarily enhance productivity, maintaining continuous Pn peaks demands substantial energy consumption, resulting in an imbalance between facility energy expenditure and growth benefits[6]. This discrepancy underscores the urgent need for transitioning to dynamic range regulation strategies based on crop physiological feedback. Research indicates that the dynamic changes in Pn, as a core metabolic process governing crop growth stages, can precisely quantify the effects of temperature stress in real time[7,8], thereby providing a viable solution to the aforementioned challenges. It is noteworthy that a recent study has identified an elastic region in Pn regulation[9], meaning that crop productivity remains stable when Pn decreases by approximately 20%. This discovery provides a theoretical foundation for the development of dynamic range control strategies.

Based on this elastic region theory, prior research has confirmed its applicability across various regulatory scenarios, such as irrigation and supplementary lighting[10,11]. The findings indicate that permitting Pn to vary within a moderate range not only ensures stable production but also substantially reduces temperature regulation energy consumption. In this context, the Pn prediction model is introduced, which serves as the basis for establishing dynamic temperature regulation standards[12]. Accurately identifying the temperature inflection points in the photosynthesis model has emerged as the key to optimizing regulation efficiency and maximizing crop growth.

Recently, curvature theory has been widely applied in seeking inflection points due to its ability to describe the degree of curvature

Received date: 2025-09-08 **Accepted date:** 2026-04-03
Biographies: Jinghua Xu, MS, research interest: agricultural information technology, Email: hua954@nwafu.edu.cn; **Minke Hong**, MS, research interest: agricultural information technology, Email: 2023055988@nwafu.edu.cn; **Miao Lu**, PhD candidate, research interest: agricultural information technology, Email: lunalu@nwafu.edu.cn; **Xudong Hu**, MS, research interest: agricultural information technology, Email: xdonghu2023@nwafu.edu.cn; **Pan Gao**, PhD, research interest: agricultural information technology, Email: pangao@nwafu.edu.cn.
***Corresponding author: Jin Hu**, Professor, research interest: gricultural sensors and information technology. College of Information Engineering, Northwest A&F University, Yangling, Shaanxi 712100, China. Tel: +86-13572502088, Email: hujin007@nwsuaf.edu.cn; **Qingxue Li**, Professor, research interest: intelligent agricultural system development. Information Technology Research Center, Beijing Academy of Agriculture and Forestry Sciences, Beijing 100097, China. Tel: +86-10-81128558, Email: lqx0072025@163.com.

of a curve or surface at a specific point[13]. Gao et al.[14] constructed the Pn surface under the interaction between light and CO_2, and employed the U-chord algorithm to calculate the maximum curvature point of the discrete curve. This approach enables the exploration of target knee points to coordinate the regulation of light and CO_2. However, despite the U-chord algorithm's robust anti-rotation and anti-noise properties, which make it ideal for feature point calculation in two dimensions, it does not fully capture the three-dimensional morphology in space. To address this, Hou et al.[15] derived a comprehensive regulation strategy for irrigation volume and photosynthetic photon flux density (PPFD) by analyzing Pn surface with Gaussian curvature, an advanced algorithm grounded in three-dimensional curvature theory. Gaussian curvature possesses a distinct geometric interpretation and serves as an inherent property of any surface, effectively capturing the surface's variations[16]. Nevertheless, its inherent global nature might pose challenges in pinpointing local feature points on the surface. Since the Pn response surface encompasses the impacts of various factors, a thorough analysis of this multidimensional surface is essential for precisely pinpointing the key points when determining the optimal regulation ranges. This study innovatively integrates the strengths of the two algorithms to more accurately divide the temperature regulation ranges of the multiple growth stages of crops.

This paper proposes a novel method to determine optimal temperature regulation ranges across growth stages of greenhouse peppers, incorporating Gaussian curvature and U-chord algorithms to address the mismatches between temperature requirements at different growth stages and actual ambient temperatures. First, a Pn prediction model was established using GA-BPNN, and the corresponding Pn response surfaces were generated through mathematical derivation. Subsequently, an innovative approach integrating Gaussian curvature analysis with the U-chord algorithm was developed to accurately capture the curvature variation trends on the Pn response surfaces, thereby enabling precise quantification of Pn's responsiveness to environmental factors. Building upon this, the random restart hill-climbing algorithm was employed to dynamically analyze curvature changes, facilitating the automatic and objective identification of critical temperature regulation boundary points. This study represents the first application of analysis based on multiple curvature metrics in crop environmental regulation, achieving multi-factor coordination and phase-specific temperature management for greenhouse-grown peppers.

2 Materials and methods

2.1 Experimental materials and data acquisition

'Zhenyan' pepper was chosen as the sample, and a nested experiment was conducted from August 16 to October 4, 2023. The experimental samples were germinated and cultivated in 72-well seed trays. Once they reached the stage of two-leaf and one-cotyledon, they were transferred to seedling cups with dimensions of 20 cm in diameter and 16 cm in height, and cultured continually in the RGL-P500D-CO_2 climate chamber (Dasikate, Hefei, China). The climate was set at 25°C for a 12-h daylight duration and 20°C for a 12-h night duration. The humidity was consistently regulated at 50% throughout the day, while the CO_2 concentration was kept at 400 μmol/mol. After a week of seedling recovery, the Pn of peppers was measured by a Li-6800 portable photosynthesis system (LI-COR, USA) under the influence of various environmental factors during the multiple growth stages. During the measurement, the pepper leaves were clamped in the leaf chamber of the Li-6800. The Pn measurement experiment diagram is shown in Figure 1.

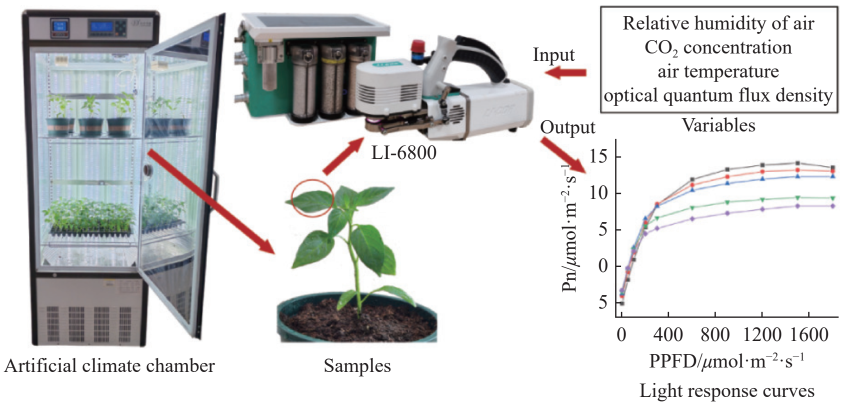

Figure 1 Measurement experiment process of Pn

By comprehensively controlling temperature, light intensity (PPFD), and CO_2 concentration across the consecutive critical growth stages (seedling, flowering, pre-fruiting, mid-fruiting, and final-fruiting) of the same batch of plants, an actively constructed multi-dimensional environment-physiological response dataset comprising 1000 data points (5×5×10×4=1000) was generated, as detailed in Table 1. This continuous cross-period nested combined experiment of environmental factors enhanced data acquisition efficiency and effectively replicated the complex and dynamic environmental interaction scenarios that crops may encounter throughout their life cycle. It thereby directly supported the engineering requirements for greenhouse environmental regulation.

2.2 Photosynthetic rate prediction model

2.2.1 Data preprocessing

The dataset was constructed by utilizing the four-dimensional characteristics of CO_2 concentration, stage, temperature, and PPFD as input vectors, with Pn serving as the output vector, as illustrated in Equation (1).

$$(X_1,Y_1),(X_2,Y_2)\cdots,(X_n,Y_n) \tag{1}$$

where, X_i=[x_i^1, x_i^2, x_i^3, x_i^4] (i=1, 2, 3, …, n, n=1000), x_i^1, x_i^2, x_i^3 and x_i^4 represent the CO_2 concentration, stage, temperature, and PPFD of the i^{th} sample, respectively. Y_i=[y_i], represents the true Pn value of the i^{th} sample.

Table 1 Setting of environmental factors

Environmental factors	Variable values
Temperature/°C	20, 24, 28, 32, 36
PPFD/μmol·m^{-2}·s^{-1}	0, 50, 100, 200, 300, 600, 900, 1200, 1500, 1800
CO_2 concentration/μmol·mol^{-1}	300, 600, 900, 1200

This study employed a normalized data preprocessing method to eliminate significant deviations caused by unit differences and dimensional variations among the variables, and uniformly converted the aforementioned environmental variables to the range of [0.2, 0.8], as shown in Equation (2)[17]. Finally, the data was randomly divided into a training set and a test set at a 7:3 ratio, with the training set used to train the Pn model and the test set used to evaluate the model's generalization ability.

$$x^{i'} = \frac{0.6 \times (x^i - x^i_{\min})}{x^i_{\max} - x^i_{\min}} + 0.2 \tag{2}$$

where, x' is the normalized data, x^i is the measured data, $x^i_{\min}$ is the minimum value of the measured data, and $x^i_{\max}$ is the maximum value of the measured data.

2.2.2 Model construction

Backpropagation neural network (BPNN) continuously refines the weights and thresholds of its network through the backpropagation mechanism, thereby achieving regression prediction for the dataset. It demonstrates superior performance when handling medium datasets, a finding corroborated by Song et al.[18] Consequently, this paper utilized BPNN to construct the Pn prediction model due to its intuitive structure and effective capture of complex effects. To comprehensively evaluate the efficacy of BPNN in Pn prediction, a comparative analysis was also conducted with support vector regression (SVR) and polynomial regression (PR), both of which are frequently employed in Pn prediction.

The BPNN architecture was implemented using TensorFlow (v2.11.0), featuring a three-layer feedforward structure comprising an input layer (4 nodes), a single hidden layer (10 nodes), and an output layer (1 node). The model was trained using backpropagation with mean squared error (MSE) as the loss function. The learning rate was set to 0.01, and training proceeded for 1000 epochs or until convergence. The specific calculation process is shown in Equation (3).

$$f(X) = g\left(\sum_{j=1}^{k} h\left(\sum_{i=1}^{n} w_{ij}x_i + b_j\right) w_{jk} + b_k\right) \tag{3}$$

where, the weights w_{ij} and w_{jk} denote those between the hidden layer and the input layer, and the hidden layer and the output layer, respectively. Similarly, b_j and b_k represent the thresholds for these connections. k stands for the number of input variables, while n represents the amount of data. $h(\cdot)$ is the Sigmoid activation function, which compresses the output to the range [0,1]. $g(\cdot)$ is the ReLU transfer function.

SVR and PR were employed as comparative models against BPNN to enable systematic performance evaluation. SVR employed kernel functions to address nonlinear relationships by transforming low-dimensional nonlinear problems into high-dimensional linear space[19]. The model utilized a radial basis function (RBF) kernel for Pn prediction, with hyperparameters optimized through grid search methodology. PR, a widely-used predictive approach[20], was implemented using a four-variable quartic polynomial regression. The model simplified complexity by focusing on temperature's highest-order term as the primary effect while incorporating temperature-factor interactions.

To enhance model robustness and improve convergence efficiency, a genetic algorithm (GA) was employed for parameter tuning. The parameters to be optimized included the initial weights and thresholds of BPNN, the penalty parameter c and kernel function parameter g of SVR, and the coefficients a_i of PR. The BPNN optimization process was taken as an illustrative example, and its corresponding flowchart is depicted in Figure 2. Among them, GA defined population size S=100, genetic generation G=50, crossover probability P_x=0.5, mutation probability P_c=0.2, and the number of mutated genes per chromosome M=3[21].

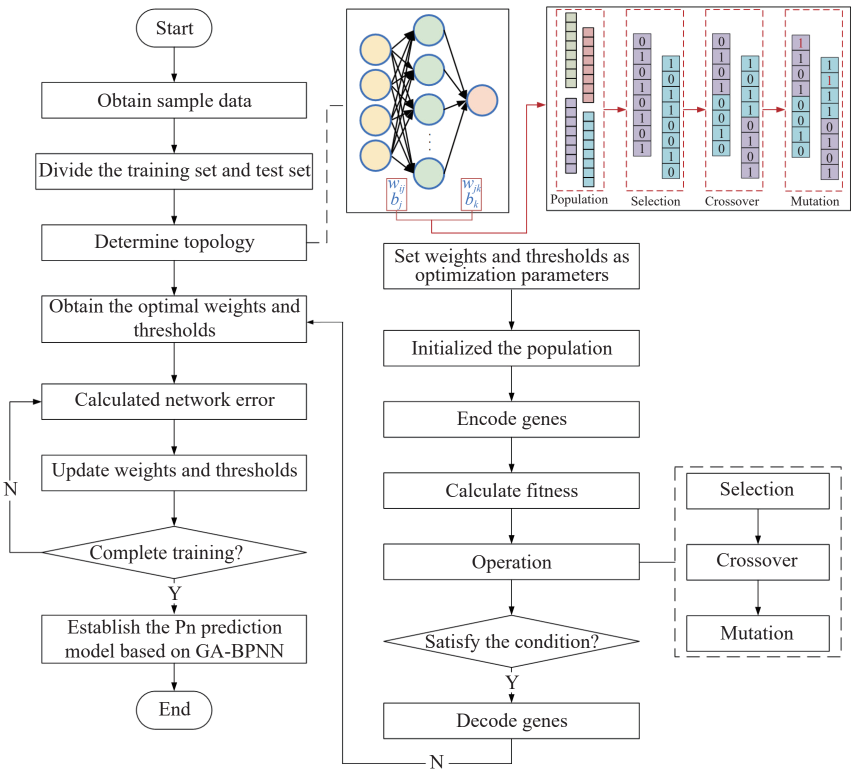

Figure 2 Flowchart of the BPNN algorithm optimized by GA

This study aimed to determine the optimal temperature ranges for various growth stages of pepper plants to enhance agricultural production efficiency. To evaluate the influence of temperature on the Pn of peppers, the Pn response surfaces were constructed during specific growth periods and CO_2 concentration conditions. These response surfaces characterized Pn as a function of PPFD and temperature, as defined in Equation (4). These Pn response surfaces were presented in a three-dimensional graphical form. In these surfaces, the *X*/*Y* axes corresponded to the environmental factors PPFD and temperature, while the *Z* axis represented the predicted photosynthetic rate output by the model. This visualization reflected the variation patterns of Pn under the interactive effects of the factors.

$$\vec{f}(x^1, x^2) = f(X)|_{x^3=T, x^4=\text{PPFD}} \tag{4}$$

where, $\vec{f}(\cdot)$ represents the sub-model for deriving Pn in the photosynthetic rate prediction model.

2.2.3 Model evaluation

To measure the performance and training effect of the model, evaluation indices such as root mean square error (RMSE), maximum absolute error (MAE), and coefficient of determination (R^2) were used to evaluate the performance of the model, as shown in Equations (5)-(7)[22].

$$\text{RMSE} = \sqrt{\frac{1}{n}\sum_{i=1}^{n}\left[Y_i - f(X_i)\right]^2} \tag{5}$$

$$\text{MAE} = \max\{|Y_i - f(X_i)|\},\ i = 1, 2, ..., n \tag{6}$$

$$R^2 = \frac{\sum_{i=1}^{n}\left[f(X_i) - \frac{1}{n}\sum_{i=1}^{n} Y_i\right]}{\sum_{i=1}^{n}\left[Y_i - \frac{1}{n}\sum_{i=1}^{n} Y_i\right]} \tag{7}$$

where, n is the number of data points, and $f(\cdot)$ is the predicted value of the Pn model.

2.3 Determination of optimal temperature regulation ranges

2.3.1 Gaussian curvature calculation for Pn response surface

Since photosynthesis plays an important role in crop biomass accumulation, either too high or too low temperature will affect crop yield[23]. To determine the optimal growth temperature for peppers during various stages, the Gaussian curvature model was used to calculate the curvature change of corresponding Pn response surfaces[24]. This approach significantly enhanced the fault tolerance and stability of environmental dynamic regulation, allowing for a more in-depth identification of the robust trend of Pn in response to environmental changes, and thus enabling the determination of the optimal growth temperature range for crops.

The Pn response surfaces were constructed using PPFD and temperature as the x and y coordinates, respectively. These surfaces comprehensively integrated the influence of multiple factors, including temperature, PPFD, CO_2 concentration, and growth stages on Pn. They revealed the law of Pn's change and provided guidance for identifying appropriate temperature target ranges. Gaussian curvature is mainly used to describe the degree of curvature or shape characteristics at a certain point on the surface. Higher values corresponded to greater surface curvature, while lower values indicated flatter surface regions[25]. Therefore, this study leveraged the Gaussian curvature to explore the curvature changes of the Pn response surface, laying a foundation for determining the target temperature ranges.

The Gaussian curvature of Pn response surfaces was determined by discretizing the surface into discrete points, followed by curvature computation at each point. According to the design range of the experiment, the temperature dispersion range was 20°C-36°C, the distance step size was set to 0.1°C, and the discrete set was $T=\{t_i\}$, $t_i=20+0.1i$, $i=0, 1, 2, …, 160$. Since the light compensation point of pepper was generally between 50-100 μmol/(m²·s), the dispersion range of PPFD was set to 100-1800 μmol/(m²·s) with a step size of 10 μmol/(m²·s), and the discrete set was $P=\{p_j\}$, where $p_j=100+10j$, $j=0, 1, 2, ..., 170$. A total of 27 531 discrete points were generated per Pn response surface through this discretization process.

Three-dimensional data normalization was conducted to address the significant magnitude disparities among temperature, PPFD, and Pn parameters. This preprocessing enhanced the stability of curvature computations. Subsequently, the Gaussian curvature at each point was computed, resulting in the construction of Gaussian response surfaces. For computational analysis, point P on the normalized Pn response surface was defined with four adjacent base points corresponding to its neighboring surface positions. The geometric configuration approximated point P as infinitesimally proximal to the base surface. Adjacent triangles were formed between point P and its surrounding nodes, as illustrated in Figure 3. The Gaussian curvature K at point P was ultimately determined through angular summation and triangular area calculations using Equations (8)-(10)[26].

$$K = \frac{1}{A}\left(2\pi - \sum_{i=1}^{N}\theta_i\right) \tag{8}$$

$$A = \sum_{i=1}^{N}\sqrt{s(s-l_i)(s-l_{i+1})(s-m_i)} \tag{9}$$

$$\theta_i = \arccos\left[\frac{l_i^2 + l_{i+1}^2 - m_i^2}{2l_i l_{i+1}}\right] \tag{10}$$

where, N is the number of triangles with vertices and adjacent points, and A is the sum of the areas of all triangles. Take the triangle formed by points P, v_i, and v_{i+1} as shown in Figure 3, θ_i represents the apex angle of the ith triangle. The side lengths of this triangle are denoted as l_i, l_{i+1}, and k_i, while $s=(l_i+l_{i+1}+k_i)/2$ signifies the semi-perimeter of the triangle that intersects at point P. If the local surface area around vertex P is flat, meaning point P lies coplanar with points v_i and v_{i+1}, then the Gaussian curvature value is 0. When the Gaussian curvature value is positive, the discrete surface resembles an ellipsoid. Conversely, if the Gaussian curvature value is negative, the discrete surface takes the shape of a saddle.

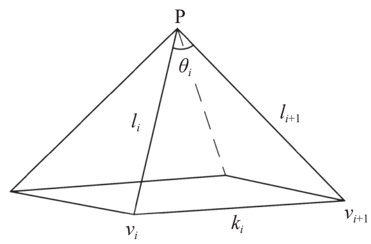

Figure 3 Schematic diagram for calculating Gaussian curvature

2.3.2 Temperature target boundaries calculation

The Gaussian response surfaces were able to reveal the response patterns of Pn to temperature changes under different conditions, and these universal principles provided an important basis for defining the target regulation boundaries. To accurately and intuitively identify the temperature regulation boundaries, the

Gaussian response surfaces were first instantiated with an increment of 50 μmol/(m^2·s) in PPFD, thereby obtaining T-G response curves for various light intensity levels. The input of T-G response curves is temperature, and the output is the curvature value. Subsequently, the input and output were normalized using Equation (2) to eliminate the magnitude difference. According to the law of the response function, any point on the response curve was set as M_i, and its U-chord curvature was calculated. Two adjacent points M_j and M_k were generated via symmetric translation by equal distances along the coordinate axes relative to point M_i. These points preserved a Euclidean distance u from M_i and satisfied the geometric constraints in Equations (11) and (12), as illustrated in Figure 4.

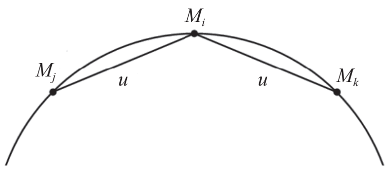

Figure 4 Schematic diagram of U-chord curvature calculation

$$\|M_jM_i\| = u \tag{11}$$

$$\|M_iM_k\| = u \tag{12}$$

where, u stands for topological distance, $0<u<1$.

Once the points M_j and M_k were found, the support domain [M_j, M_k] of M_i could be obtained. Then the cosine associated with the angle between the front and rear arm vectors within the support domain [M_j, M_k] of M_i was calculated as a measure of discrete curvature. At this time, the discrete curvature of point M_i is shown in Equation (13).

$$c_i = s_i\sqrt{1-\left(\frac{\|M_jM_k\|}{2u}\right)^2} \tag{13}$$

where, $s_i = sign[(x_i - x_k)(y_j - y_k) - (x_j - x_k)(y_i - y_k)]$ is the symbol of the discrete curvature value; (x_i, y_i), (x_j, y_j), (x_k, y_k) represent the coordinates of the points M_i, M_j, M_k respectively.

The U-chord values of T-G response curves quantified the variation in Gaussian curvature and served as a metric derived from the target boundaries. Based on these U-chord values, the reasonable upper and lower boundaries on both sides of the peak of the response curve were selected, so as to reach the target ranges of temperature regulation. Due to the physiological phenomena of peppers, the curvature trends on both sides of the peak were different. Therefore, the random restart hill-climbing method was adopted to obtain the upper and lower boundary points that were optimal for temperature regulation targets according to the two strategies of Equation (14) and (15) respectively. Finally, by mapping the obtained points onto the response surface of the Pn prediction model, the corresponding temperature regulation ranges were determined.

$$c_i^- > c_i < c_i^+ \tag{14}$$

$$c_j^- > c_j > c_j^+ \tag{15}$$

where, c_i and c_j represent the U-chord values of the Gaussian curvature of the upper and lower boundary points respectively; c_i^- and c_i^+ denote arbitrary points located on the left and right sides of c_i, respectively, while c_j^- and c_j^+ denote arbitrary points located on the left and right sides of c_j, respectively.

2.4 Model validation

From August 18 to October 18, 2024, the long-term culture validation experiment was completed on samples of 'Zhenyan' peppers cultured to flowering stage to evaluate the effect of the optimal temperature range determined in this study on the growth of peppers. Among the five growth stages of peppers, the seedling stage is crucial for root development, leaf formation, and nutrient accumulation. It is extremely susceptible to temperature, which directly impacts their yield and quality. Upon entering the flowering stage, the growth focus of pepper shifts from vegetative growth to reproductive growth, resulting in a deceleration of branch and leaf expansion[27]. Consequently, morphological and physiological phenotypes, including plant height, stem diameter, dry weight, fresh weight, leaf area, and the seedling vigor (Equation (16)), were employed to assess the growth of peppers during the seedling stage[28,29]. Additionally, the number of flowers and fruits, the days required for flowering and fruiting, as well as the dry and fresh weights of the fruits were utilized as evaluation indicators for both the flowering and fruiting stages[30,31].

The experiment comprised one experimental group and two control groups. Utilizing data from the summer solar greenhouse at Jingyang Vegetable Experimental Demonstration Station of Northwest A&F University in China, an artificial climate chamber was employed to simulate environmental changes. This simulation environment, designed based on real greenhouse data, ensures that the scenarios in the verification tests possess a high degree of representativeness. Consequently, its results can directly inform the development of actual greenhouse control strategies. The control stage was set from 8:00 to 20:00. Temperature and PPFD were adjusted every 2 h, while the average CO_2 concentration during the initial 15 min served as the model input[32]. This control frequency evaluates the model's capability to capture changes in the greenhouse environment while maintaining stability, and it represents a crucial approach to addressing the uncertainty inherent in real-world environmental monitoring data. Figure 5 shows the environmental controls for the first five days. The experimental group strictly followed the optimal temperature ranges determined in this study and regulated the ambient temperature to this optimal level for pepper cultivation. One control group was cultivated in a climate chamber to simulate greenhouse temperature fluctuations shown in Figure 5, while the other control group was set at a fixed temperature of 25°C[33]. All other environmental variables for the three groups were kept consistent with those recorded during data collection. The planting situations under the three strategies are shown in Figure 6. These subfigures visually present the phenotypic differences of pepper plants under the three distinct management approaches. The above-mentioned indices were analyzed using Minitab 2022 software.

$$\mathrm{SV} = \left(\frac{S}{H} + \frac{\mathrm{RDW}}{\mathrm{SDW}}\right) \times \mathrm{TDW} \tag{16}$$

where, S stands for stem diameter, H stands for plant height, RDW stands for root dry weight, SDW stands for shoot dry weight, and TDW stands for total dry weight.

3 Results and analysis

3.1 Experimental data characteristics

Drawing upon experimental data, the influence of temperature on Pn under different stages and environmental factors was explored and presented in the form of light response curves, as shown in Figure 7. Comparative analysis revealed significant variations in light response curves across different growth stages, with temperature being a critical factor influencing photosynthetic characteristics. Under low CO_2 concentration (300 mol/mol), the flowering stage exhibited more clustered light response curves compared to other stages, with Pn differences between adjacent temperature gradients (4°C) remaining below 1 μmol/(m^2·s), demonstrating enhanced thermal adaptability (20°C-32°C). In contrast, other growth stages, particularly the seedling stage, showed greater curve dispersion (2.5-fold higher than that of the flowering stage). When temperatures exceeded 32°C under a PPFD≥800 μmol/(m^2·s), seedling-stage Pn decreased by 83.24% on average compared to 28°C conditions, indicating heightened environmental sensitivity. At elevated CO_2 (900 μmol/mol), warming synergistically enhanced photosynthetic capacity, manifested by 10-16 μmol/(m^2·s) Pn increments and expanded light-response curve distributions. This CO_2-temperature interaction substantially alleviated high-temperature/strong-light co-inhibition, particularly in seedling and mid-fruiting stages. Concurrently, plants developed enhanced temperature sensitivity that effectively buffered thermal fluctuations. These dynamically coordinated thermal responses establish a critical framework for precision modeling of photosynthesis mechanisms under climate change scenarios.

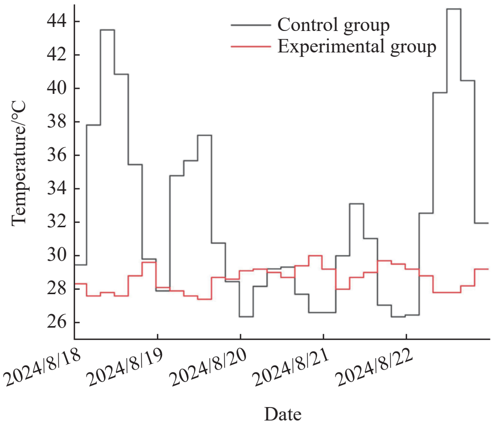

a. The change curve of temperature

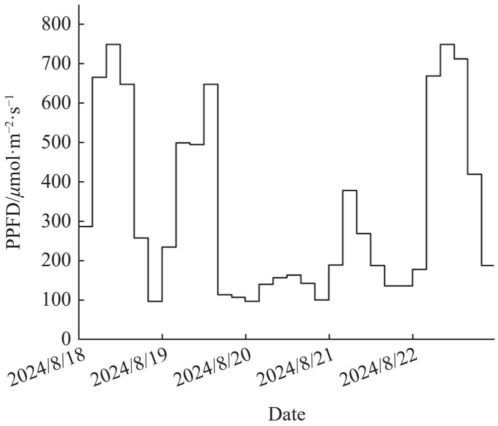

b. The change curve of PPFD

Figure 5 The change curve of temperature and PPFD of simulated greenhouse

a. Optimal ranges b. Fixed threshold c. No-operation

Figure 6 The planting situations under the three strategies

3.2 Results and analysis of the Pn prediction model

The Pn at various growth stages is predicted utilizing BPNN, SVR, and PR, along with their GA-optimized versions. The predictive performance of these models is assessed based on the RMSE, MAE, and R^2, with comprehensive results presented in Table 2. Among these methods, GA-BPNN demonstrated superior performance across all metrics, achieving the highest R^2 value (0.9812) and the lowest RMSE and MAE [1.35 μmol/(m^2·s) and 0.89 μmol/(m^2·s), respectively]. GA-SVR performs second best, while PR shows the least effectiveness. Furthermore, the fitting slope of the GA-BPNN model is 0.9752, indicating that its prediction outcomes more closely align with the ideal scenario (1:1 line). These results suggest the robust nonlinear mapping capability of BPNN, which, when optimized by GA, can achieve higher prediction accuracy. Compared with models proposed by other researchers[34,35], the GA-BPNN model not only meets the accuracy requirements for theoretical calculations but also lays a solid foundation for its universal application. This provides a solid theoretical foundation for determining the optimal growth temperature ranges in future studies.

The above results indicate that compared with other models, the GA-BPNN model demonstrated better performance in terms of prediction accuracy and applicability, making it more suitable for subsequent research on temperature regulation ranges. To intuitively display the prediction performance of GA-BPNN, the Pn response surfaces are shown in Figure 8. Figure 8a and 8b illustrate the Pn predictions at the flowering stage with a CO_2 concentration of 600 μmol/mol and at the pre-fruiting stage with a CO_2 concentration of 900 μmol/mol, respectively.

Despite variations in Pn trends across different stages and environmental conditions, it is worth noting that Pn changes tend to be positively correlated with temperature changes. This suggests that within the highest temperature set in this study (36°C), the photosynthetic enzymes did not undergo denaturation or inactivation. However, as the temperature increased, the rate of increase in Pn gradually slowed, indicating that the photosynthesis of peppers was inhibited by high temperatures. Therefore, deeply exploring the potential variation patterns of Pn during different growth stages of peppers is crucial for rationally planning the appropriate temperature regulation ranges.

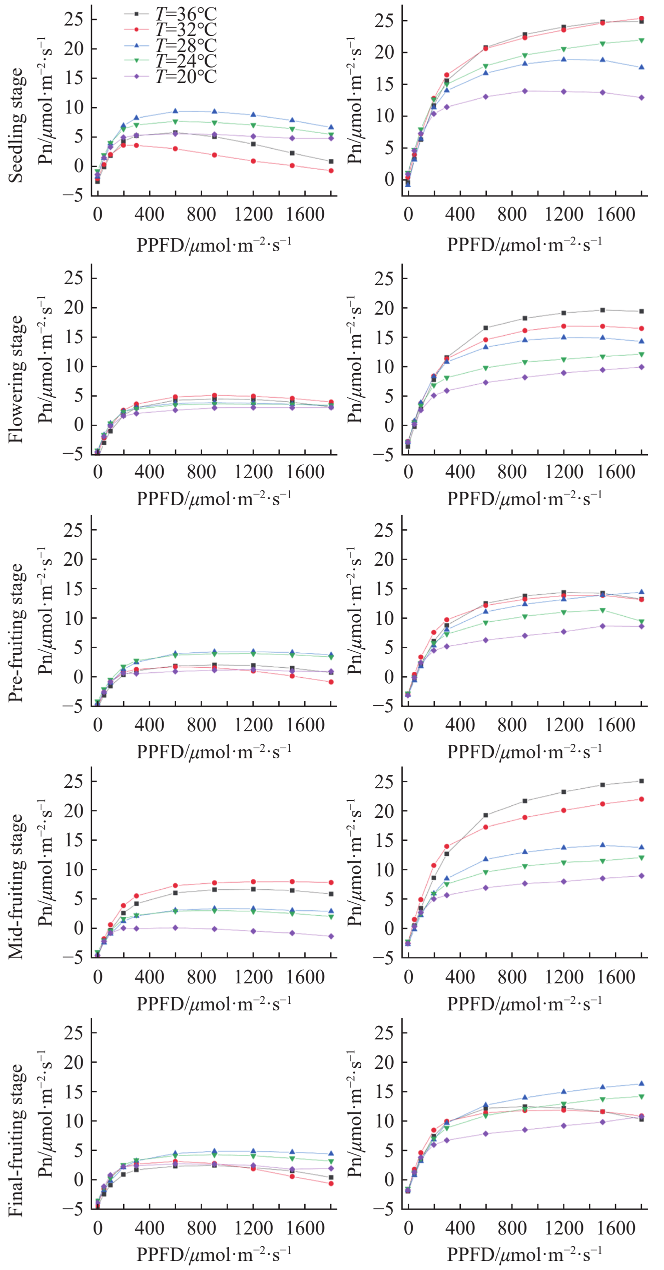

a. CO_2 concentration of 300 μmol/mol b. CO_2 concentration of 900 μmol/mol

Figure 7 Light response curves

3.3 Results and analysis of the optimal temperature ranges

3.3.1 Results and analysis of Gaussian curvature

Scientific temperature management is crucial for effective pepper cultivation. To comprehensively investigate the global patterns of pepper's Pn in response to temperature changes, the Gaussian curvature of the Pn response surfaces was calculated, which helped construct a Gaussian response surface model. This aims to quantify and reflect the curvature characteristics of the Pn response surfaces, as illustrated in Figure 9. The model provides an intuitive visualization of the Gaussian response characteristics of pepper's Pn response surfaces under varying conditions. Figure 9 depicts the Gaussian response surfaces and their corresponding heatmaps under two CO_2 concentrations: 600 μmol/mol (flowering stage) and 900 μmol/mol (pre-fruiting stage).

Table 2 Comparison of algorithm test set evaluation

Modeling approaches	RMSE/ μmol·m^{-2}·s^{-1}	MAE/ μmol·m^{-2}·s^{-1}	R^2	Fitting equation
GA-BPNN	1.35	0.89	0.9812	y=0.9752x+0.4438
GA-SVR	1.69	1.18	0.9438	y=0.9559x+0.2430
GA-PR	2.40	1.93	0.9126	y=0.9266x+0.6697
BPNN	1.53	1.09	0.9541	y=0.9671x+0.0800
SVR	2.00	1.40	0.9229	y=0.9202x+0.0853
PR	3.18	2.55	0.8109	y=0.7968x+2.0608

Figure 9a presents Gaussian response surfaces under different environmental conditions and stages, with both models exhibiting highly similar temperature response patterns in terms of shape. Figure 9b provides a quantitative analysis of curvature features, revealing that the interaction between temperature and PPFD significantly influenced the morphology of the response surfaces. When PPFD is below approximately 800 μmol/(m²·s), the Gaussian curvature is negative (K<0), showing a biphasic characteristic of first increasing and then decreasing with temperature, ultimately stabilizing to form a concave surface. Combined with the observational data from Figure 9, within this PPFD range, temperature increases (20°C-36°C) result in only a weak enhancement of Pn, with an increase not exceeding 5 μmol/(m²·s). However, the absolute curvature value can reach 0.20 or higher, indicating that temperature is not the primary limiting factor for Pn development under these conditions. The antagonistic interaction between light intensity and temperature leads to a broader temperature adaptation range for peppers, consistent with the implications of negative curvature.

Conversely, when PPFD exceeds 800 μmol/(m²·s), the Gaussian curvature gradually becomes positive (K>0), exhibiting an opposite trend with temperature compared to the low-light scenario, and the response surface transitions to a convex morphology. In this regime, Pn displays an accelerated growth pattern with rising

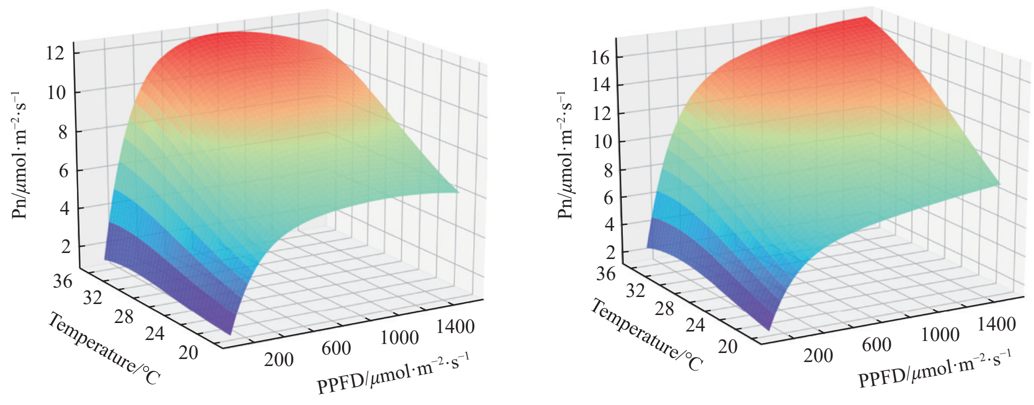

a. Flowering stage with a CO_2 concentration of 600 μmol/mol b. Pre-fruiting stage with a CO_2 concentration of 900 μmol/mol

Figure 8 Photosynthetic response surface temperature, contrasting with the low light intensity conditions. As light saturation is reached, temperature emerges as the dominant limiting factor for Pn. The high-temperature inhibition effect aligns the direction of light and temperature constraints, driving Pn growth in a convex acceleration mode. This shift enhances the temperature sensitivity of peppers and narrows their adaptive temperature range. In greenhouse environments, high light intensity often coincides with elevated temperatures, making fixed threshold regulation methods both imprecise and cost-inefficient. Balancing temperature regulation within optimal ranges by marginally sacrificing Pn becomes a critical priority for greenhouse management.

Notably, inflection points in Pn-temperature dynamics are observed within the 20°C-24°C and 32°C-36°C ranges, likely correlating with phase transition temperatures in the kinetic properties of photosynthetic enzymes. These inflection points elucidate the adaptive mechanisms of pepper photosynthesis under varying thermal conditions and hold significant implications for understanding temperature sensitivity in pepper growth. Therefore, defining the temperature regulation boundaries between 20°C-24°C and 32°C-36°C is crucial for optimizing greenhouse temperature management in pepper cultivation. This discovery establishes a robust scientific foundation for advancing precision agriculture practices in controlled environments.

However, it is important to note that Gaussian response surfaces have complex geometric shapes, and the points on the surface may exhibit varying curvatures and orientations, which makes the identification and calculation of critical boundaries difficult and resource-consuming. Meanwhile, while the Gaussian curvature method is effective in capturing the global changes in Pn, the noise present in this complex surface can interfere with the selection of feature points. This interference complicates the accurate delineation of temperature range boundaries, further impacting the precision of temperature regulation. Consequently, the introduction of the U-chord algorithm, which excels in feature point selection, becomes particularly crucial. By reducing the computational dimension, this integration enables the more accurate determination of the optimal temperature range for pepper growth, ultimately leading to more efficient and precise cultivation management.

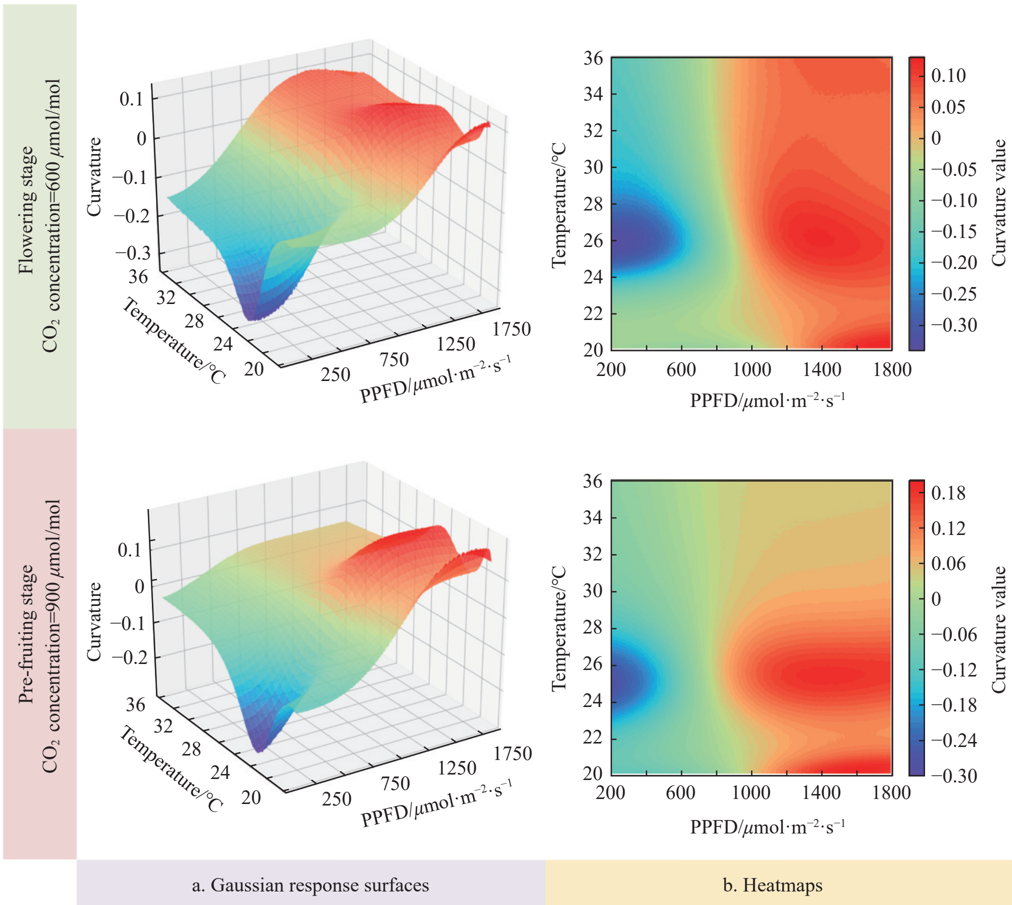

Figure 9 Gaussian response surfaces and their heatmaps

3.3.2 Results and analysis of the optimal temperature regulation ranges

To better demonstrate the prominent features of the Gaussian response surfaces and facilitate the exploration of critical boundaries, the Gaussian response surfaces were converted into multiple T-G response curves. Then, based on actual planting conditions, the points showing the maximum rate of change to the left of the peak value and the minimum rate of change to the right were selected as the upper and lower boundaries of the optimal temperature regulation range, respectively. Furthermore, the peak values corresponded to the optimal regulation temperature values. This methodology not only enhances the precision of temperature management in solar greenhouses but also facilitates the growth and development of crops. Based on this, the U-chord values were utilized as the metric for determining the upper and lower boundary points, with the results presented in Figure 10.

Figure 10 illustrates the optimal temperature ranges derived from seven distinct PPFD levels during the flowering stage with a CO_2 concentration of 600 μmol/mol and the pre-fruiting stage with a CO_2 concentration of 900 μmol/mol. Figure 10a displays the results of temperature ranges on the T-G response curves, revealing that the suitable growth temperature ranges for crops differ in various growth stages and under different PPFD conditions. Generally, as PPFD increases, the optimal growth temperature range for peppers narrows. This phenomenon occurs because strong light can induce photoinhibition in the photosynthetic system of peppers, and the combined inhibitory effect of high temperatures restricts normal crop growth[36]. Consequently, under intense light conditions, peppers exhibit greater sensitivity to temperature changes, resulting in the narrower optimal growth temperature ranges. In contrast, under weaker PPFD conditions, peppers demonstrate higher adaptability to temperature variations, leading to wider optimal temperature ranges. Figure 10b provides a two-dimensional mapping of the temperature ranges corresponding to the Pn response surfaces. The two green lines denote the upper and lower boundaries of the regulation range, while the central black dotted line with star marks represents the optimal temperature. As depicted in Figure 10b, the optimal temperature range during the pre-fruiting stage is notably narrower than that during the flowering stage. This difference arises because the transition from vegetative to reproductive growth involves more intricate nutrient distribution, making pepper plants more sensitive to temperature requirements. Excessively high temperatures may lead to elongated trunks and fruit drop[37]. This also confirms the necessity of managing pepper greenhouse temperatures according to different stages. More detailed results are presented in Table 3. It is evident that as PPFD increased from 300 μmol/(m^2·s) to 900 μmol/(m^2·s), the optimal temperature ranges generally exhibited a narrowing trend across all growth environments and stages, consistent with the findings illustrated in Figure 10. Additionally, Table 3 clearly reflects the temperature requirements of pepper plants, which necessitate slightly lower temperatures during the seedling stage to promote vegetative growth and higher temperatures during the mid-fruiting stage to enhance fruit development. This is consistent with the research results of predecessors[38]. In summary, the determined temperature ranges effectively avoid the high-temperature inhibition zone and provide a rational temperature management strategy for pepper cultivation.

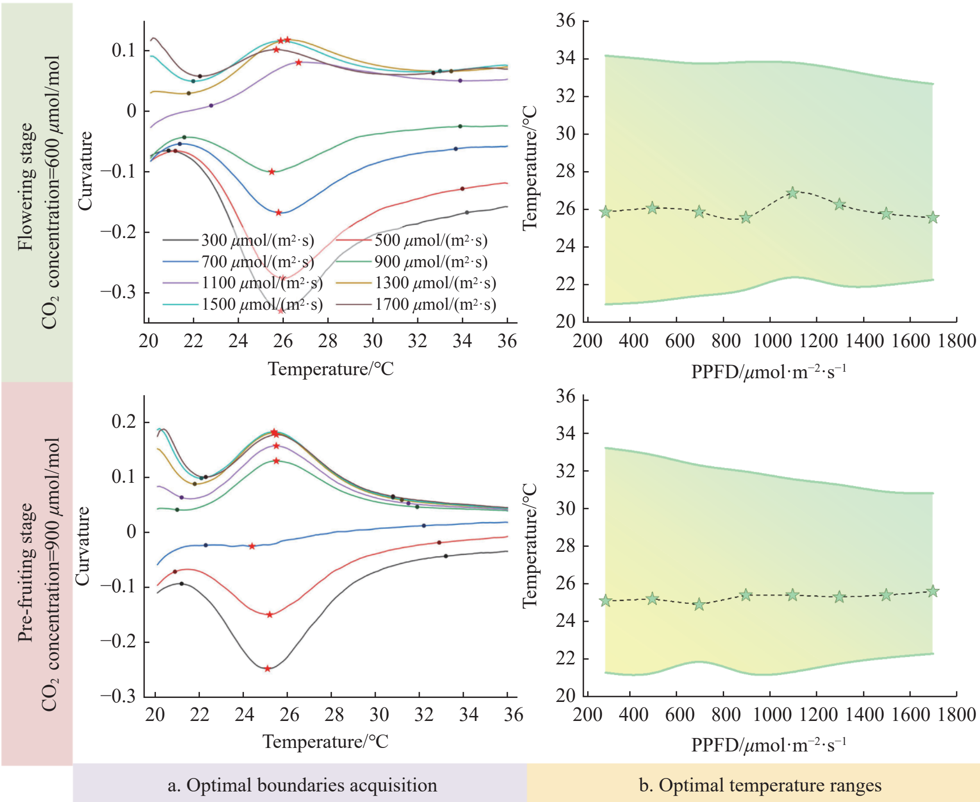

Figure 10 Results of greenhouse temperature regulation ranges

Table 3 The optimum temperature ranges under different environments and stages

CO_2/ μmol·mol^{-1}	Temperature range/°C	Seedling			Flowering			Pre-fruiting			Mid-fruiting			Final-fruiting		
		PPFD/μmol·m^{-2}·s^{-1}			PPFD/μmol·m^{-2}·s^{-1}			PPFD/μmol·m^{-2}·s^{-1}			PPFD/μmol·m^{-2}·s^{-1}			PPFD/μmol·m^{-2}·s^{-1}		
		300	900	1500	300	900	1500	300	900	1500	300	900	1500	300	900	1500
300	Max	31.4	30.0	29.6	34.5	32.3	29.7	32.3	32.4	30.1	34.6	34.0	30.2	33.4	34.3	33.3
	Min	23.0	22.5	22.3	22.3	22.8	22.6	21.4	22.8	23.1	26.0	21.6	22.2	26.7	27.7	26.3
	Optimal	25.7	25.9	26.3	28.8	27.7	26.4	28.9	28.6	26.8	30.4	30.2	27.0	29.2	28.3	27.9
600	Max	30.2	30.8	32.2	34.0	33.9	33.0	34.1	32.8	31.2	34.0	34.7	31.0	33.0	32.3	30.3
	Min	21.2	22.0	23.4	21.0	21.6	22.0	20.9	22.0	22.1	22.2	22.0	22.4	21.8	21.4	22.4
	Optimal	26.3	26.9	27.1	25.9	25.5	25.7	25.5	27.0	25.4	25.2	26.1	25.3	26.3	25.2	24.9
900	Max	31.9	31.8	32.3	31.9	31.9	30.9	32.1	29.7	31.0	32.5	31.5	31.3	30.6	30.6	31.4
	Min	21.4	21.6	22.7	21.0	21.6	21.9	21.1	22.9	21.9	21.3	21.1	22.0	20.9	21.4	21.9
	Optimal	25.8	26.2	26.5	25.4	25.4	25.6	25.0	25.6	25.4	25.1	25.3	25.4	24.8	25.1	25.7
1200	Max	32.0	32.6	30.8	31.5	31.2	31.6	31.9	31.1	31.9	30.7	31.1	31.8	31.4	31.8	31.0
	Min	21.2	21.6	22.7	21.2	21.8	22.1	21.1	22.1	22.0	21.4	21.4	22.0	21.1	21.3	21.9
	Optimal	25.7	26.1	27.1	25.3	25.7	25.9	25.0	25.6	25.6	24.9	25.5	25.6	24.8	25.1	26.0

3.4 Validation results and analysis

3.4.1 Comparison of different regulation strategies

To verify the effect of the optimal temperature ranges of peppers obtained under different environments, a theoretical comparison was conducted between the proposed research method and the fixed threshold regulation method. The results are shown in Table 4. Table 4 presents some results for a CO_2 concentration of 600 μmol/mol. According to Figure 5, PPFD typically does not exceed 1000 μmol/(m^2·s) in summer greenhouse environments, hence, Table 4 only displays PPFD results within this range. Compared with the fixed threshold method, the proposed approach in this study demonstrated optimal Pn growth rate of 6.13%, indicating that temperature regulation significantly enhances photosynthetic efficiency. However, the seedling stage exhibited paradoxical characteristics: despite showing the smallest Pn increment (merely 3.56%, significantly lower than other stages), it achieved the highest absolute Pn values among all growth phases. This phenomenon suggests that photosynthetic response thresholds to temperature variations approach saturation during seedling development, where minor thermal fluctuations may substantially impact physiological performance. Such behavior likely stems from seedlings prioritizing organogenesis over stress response mechanisms, resulting in reduced thermal tolerance elasticity and narrower adaptive temperature ranges. These findings align with data presented in Table 3.

Table 4 Comparison of optimal temperature ranges determined by this study's method versus fixed threshold method

Stage	PPFD/ μmol·m^{-2}·s^{-1}	Optimal value of the optimal ranges		Fixed threshold (25°C)	The Pn increase rate of this paper's method/%
		Optimal temperature/°C	Pn/ μmol·m^{-2}·s^{-1}	Pn/ μmol·m^{-2}·s^{-1}	
Seedling stage	300	26.3	10.59	10.36	2.22%
	500	26.6	12.40	11.99	3.42%
	700	26.7	12.86	12.35	4.13%
	900	26.9	12.84	12.29	4.48%
Flowering stage	300	25.9	5.94	5.65	5.13%
	500	26.5	8.01	7.28	10.03%
	700	26.3	8.53	7.92	7.70%
	900	25.9	8.62	8.20	5.12%
Pre-fruiting stage	300	25.5	5.30	5.14	3.11%
	500	26.1	7.36	6.82	7.92%
	700	26.7	8.40	7.63	10.09%
	900	27.0	8.98	8.09	11.00%
Mid-fruiting stage	300	25.2	5.30	5.10	3.92%
	500	25.7	7.32	6.82	7.33%
	700	26.3	8.25	7.73	7.10%
	900	26.1	8.98	8.33	7.80%
Final-fruiting stage	300	26.3	5.55	5.17	7.35%
	500	26.2	7.29	6.87	6.11%
	700	25.7	8.47	7.91	7.08%
	900	25.2	8.83	8.70	1.49%

From Table 4, it could be seen that the optimal temperature of peppers was not a single fixed value, but rather exhibited the characteristic of dynamic adjustment according to growth stages and PPFD. Within the same growth stage, the optimal temperature changed accordingly as PPFD varied. For instance, during the seedling stage, as PPFD increased from 300 μmol/(m^2·s) to 900 μmol/(m^2·s), the optimal temperature gradually rose from 26.3°C to 26.9°C. During the flowering stage, the optimal temperature fluctuated between 25.9°C and 26.5°C under different PPFD conditions; the optimal temperature in the pre-fruiting stage also increased from 25.5°C to 27.0°C as PPFD rose, and the optimal temperatures in the mid-fruiting and final-fruiting stages also adjusted correspondingly with changes in light intensity. This pattern of the optimal temperature dynamically changing with growth stages and actual environmental parameters indicated that the temperature adaptation requirement of peppers was not constant, thereby validating the necessity and feasibility of dynamically regulating greenhouse temperatures based on the crop's physiological stages and real-time environmental conditions.

3.4.2 Results of the validation experiment on environmental regulation

The present study confirmed the significant advantages of dynamic ranges regulation strategy in pepper production through systematic validation experiments. As shown in Figure 11, compared with the control groups under simulated summer greenhouse conditions (No-operation) and fixed threshold regulation, the proposed regulation strategy demonstrated enhanced adaptability and superior comprehensive benefits. Specifically, the average fresh weight of peppers in the experimental group was 63.37% higher than in the no-operation regulation group and 16.13% higher than in the fixed threshold regulation group. Similarly, the average dry weight was 78.19% higher than in the no-operation regulation group and 20.25% higher than in the fixed threshold regulation group. Regarding stem diameter and seedling vigor index, the optimal range regulation method significantly outperformed conditions without a regulation strategy. Although there was no significant difference compared to fixed threshold regulation, it demonstrated better overall effectiveness. As illustrated in Figure 11e, the pepper plants under optimal ranges regulation demonstrated maximum canopy leaf area, showing 34.83% and 23.22% increases compared to the No-operation and fixed threshold regulation conditions, respectively. These results further validate the multidimensional synergistic enhancement effects of this methodology, which proves more conducive to pepper growth. Combined with the seedling stage data presented in Table 4, although the enhancement in Pn was moderate, it exhibited significant growth-promoting effects on pepper plants. This phenomenon can be attributed to the comprehensive consideration of other environmental factors and growth stages during the selection of optimal temperature ranges, thereby improving overall photosynthetic efficiency and achieving cumulative growth benefits. These findings collectively confirm the rationality and applicability of the proposed temperature management strategy in guiding agricultural production practices.

The flowering and fruiting conditions of peppers cultivated under the three strategies are shown in Figure 12. Compared with the other two strategies, peppers grown within the optimal temperature ranges exhibit significantly enhanced flowering and fruiting performance. In Figure 12a and 12b, the mean days to flowering of this group occurred 4-7 d earlier than those under the fixed threshold and no-operation strategies. Additionally, the mean days to fruiting were shortened by 8.29 d and 14.15 d respectively compared to these two strategies. In terms of flower and fruit counts, this group demonstrated substantial advantages over the other two groups, as shown in Figure 12c and 12d. Comparative analysis reveals that the fixed threshold strategy prolonged the plant growth cycle, whereas the no-operation environment disrupted the growth dynamics of peppers, leading to an imbalance characterized by excessive vegetative growth at the expense of reproductive development. This imbalance resulted in delayed flowering and fruiting as well as a high incidence of flower and fruit abscission. In addition, Figure 12e-12f further demonstrate the superior fruit quality achieved through optimal temperature ranges regulation. The experimental group exhibited a 225.57% increase in mean fresh fruit weight compared to the no-operation regulation, along with a 91.53% enhancement over the fixed threshold group. Correspondingly, dry weight increased by 243.65% and 96.84% relative to these two baselines, respectively. These findings confirm that maintaining optimal temperature ranges not only accelerates pepper phenology (shortened growth cycles) but also improves reproductive outcomes through elevated flower/fruit production and enhanced fruit biomass. Collectively, the evidence positions this strategy as a scientifically validated approach for optimizing protected pepper cultivation systems.

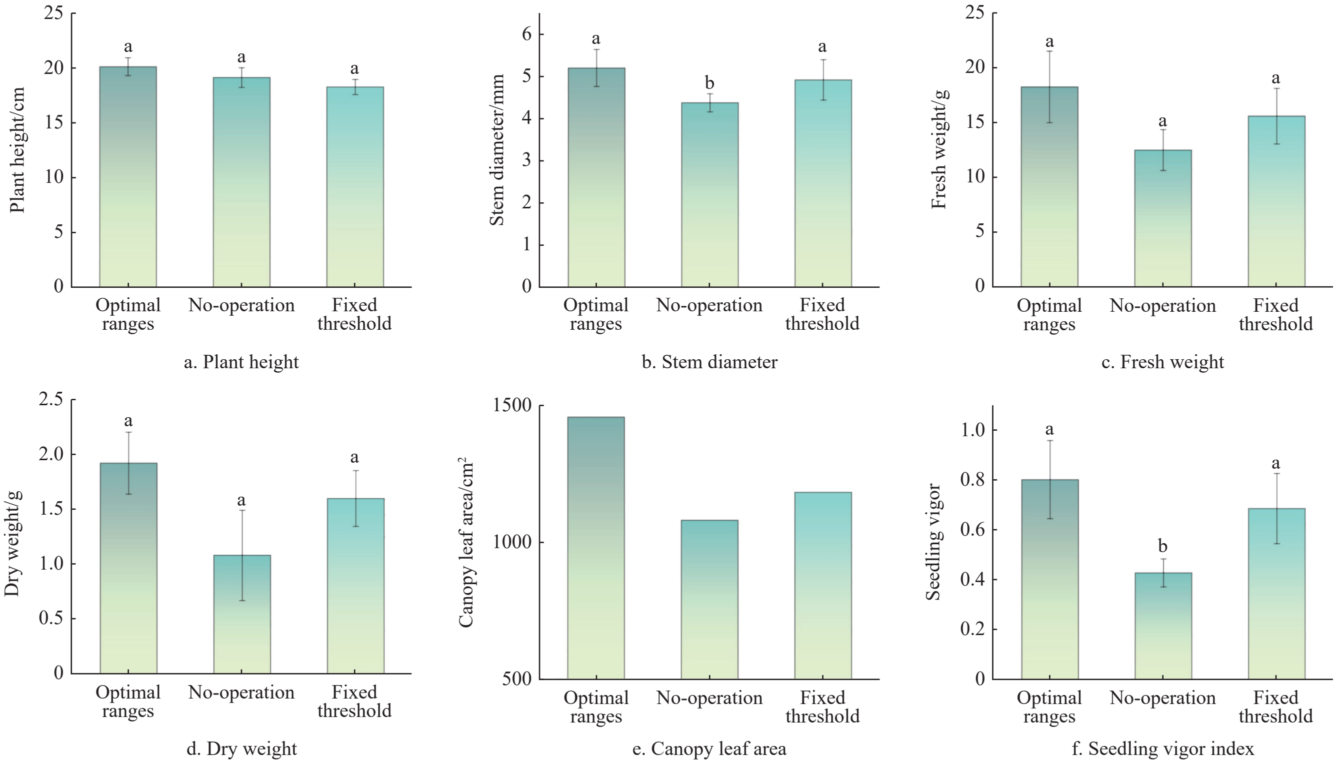

a. Plant height b. Stem diameter c. Fresh weight
d. Dry weight e. Canopy leaf area f. Seedling vigor index

Figure 11 Comparison and significance analysis results of pepper biomass under different regulation strategies

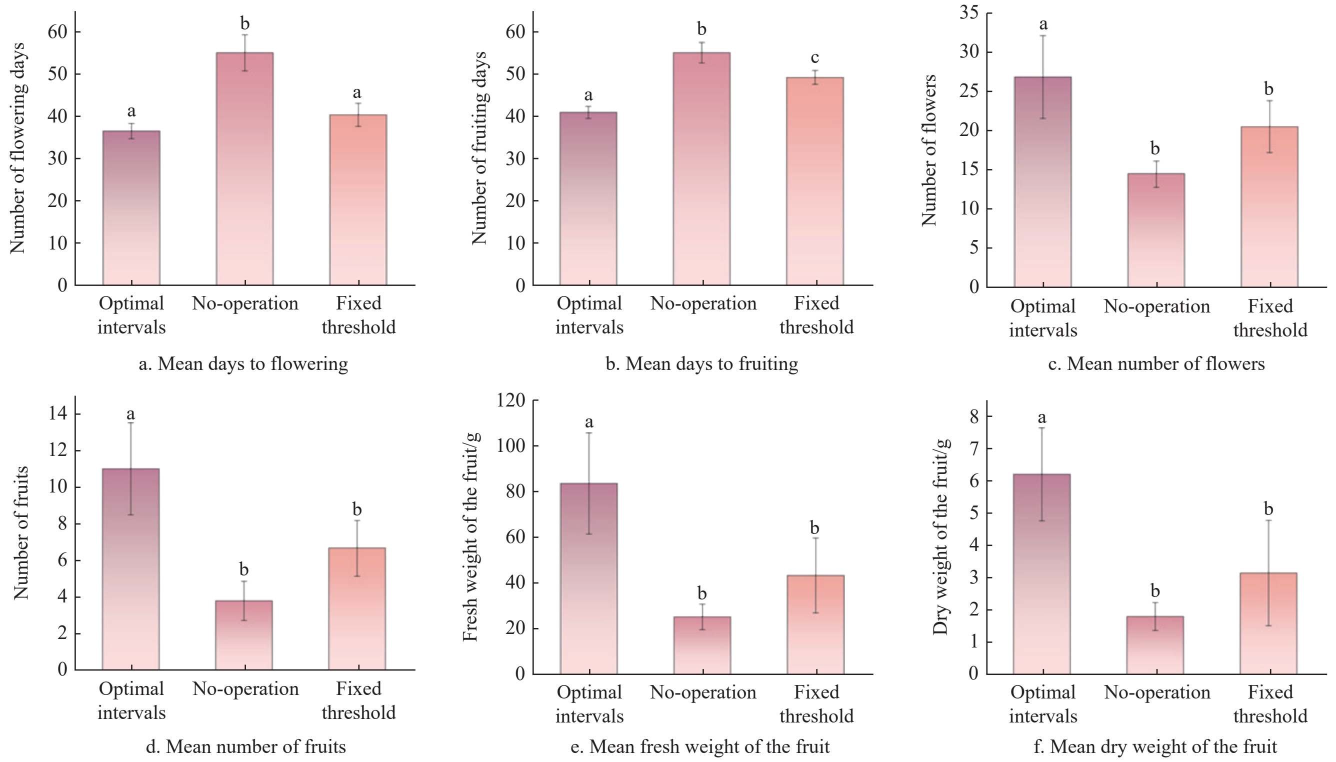

a. Mean days to flowering b. Mean days to fruiting c. Mean number of flowers
d. Mean number of fruits e. Mean fresh weight of the fruit f. Mean dry weight of the fruit

Figure 12 Comparison of flowering and fruiting situations of peppers under three regulation strategies (The number of days to flowering and fruiting started from the two-leaf and one-cotyledon stage)

4 Conclusions

In this study, a method for determining the optimal growth temperature regulation ranges for greenhouse peppers throughout their multiple growth stages was proposed by integrating Gaussian curvature and U-chord curvature algorithms. Rigorous testing validated the effectiveness and universality of this approach, providing a robust framework for planning suitable planting environments for different growth stages of peppers and establishing guidelines for temperature regulation in greenhouse cultivation.

Firstly, nested experiments were conducted to measure the Pn of peppers across their multiple growth stages under various environmental conditions. Then a Pn prediction model was established using growth stages, temperature, CO_2 concentration, and PPFD as inputs, resulting in a Pn response surface. Among the models compared, the GA-BPNN prediction model exhibited the best performance, with an R^2 of 0.9812, an RMSE of 1.35 μmol/(m^2·s), and an MAE of 0.89 μmol/(m^2·s) for the test set. Subsequently, the Gaussian curvature of the Pn response surface was calculated, constructing a Gaussian curvature response surface. Their heatmaps were plotted to quantify the interactive effects of temperature and PPFD on the variation of Pn response surfaces, thereby elucidating the common patterns of temperature impacts on Pn under different PPFD levels. Next, to accurately and intuitively identify boundary characteristic points of the optimal ranges, Gaussian response surfaces were systematically parameterized using 50 μmol/(m^2·s) PPFD increments, from which T-G response curves were derived. Using the U-chord curvature value as a metric, the key boundaries of the appropriate regulation ranges were determined using the random restart hill-climbing method. Finally, the effectiveness of the three regulatory strategies was validated. Quantitative analyses revealed that the experimental group achieved 63.37% greater fresh plant weight than the no-operation control and a 16.13% increase compared with the fixed threshold regulation group. The dry weight also increased by 78.19% and 20.25% respectively. Notably, dry fruit biomass under optimal regulation exhibited a 243.65% increase versus no-operation conditions and 96.84% improvement compared to fixed threshold regulation. It was proved that this approach not only enhanced the growth of peppers but also exhibited greater tolerance in regulation. This indicates that, in the actual operation of greenhouses, when confronted with inevitable environmental fluctuations or control errors, this method can more stably maintain the high-yield performance of crops and mitigate yield risks associated with imprecise regulation.

This research method aligns peppers growth stages with their optimal temperature ranges, offering theoretical support for greenhouse ventilation decision-making. Simultaneously, the established temperature regulation strategy provides an environmental basis for optimizing and regulating key environmental parameters such as CO_2 concentration, PPFD, soil moisture, and photostage. It is worth noting that the current research primarily focuses on the precise regulation of the single factor of temperature. Revealing the synergistic mechanisms between temperature and other environmental factors, and subsequently establishing a multi-environmental factor coupling regulation model, will constitute the focal point of future research.

Acknowledgements

This work was supported by the National Key Research and Development Program of China (CN) (Grant No. 2024YFD2001004-02), the Shaanxi Key Research and Development Program (CN) (Grant No. 2023-ZDLNY-66), and the China Postdoctoral Science Foundation (Grant No. 2024M762637).

[References]

[1] Zou Z Y, Zou X X. Geographical and ecological differences in pepper cultivation and consumption in China. Frontiers in Nutrition, 2021; 8: 718517.

[2] Rajametov S N, Lee K, Jeong H B, Cho M C, Nam C W, Yang E Y. The effect of night low temperature on agronomical traits of thirty-nine pepper accessions (*Capsicum annuum* L.). Agronomy-Basel, 2021; 11(10): 1986.

[3] Xia S B, Nan X N, Cai X, Lu X M. Data fusion based wireless temperature monitoring system applied to intelligent greenhouse. Computers and Electronics in Agriculture, 2022; 192: 103576.

[4] Carotti L, Graamans L, Puksic F, Butturini M, Meinen E, Heuvelink E, et al. Plant factories are heating up: hunting for the best combination of light intensity, air temperature and root-zone temperature in lettuce production. Frontiers in Plant Science, 2021; 11: 192171.

[5] Wang Y L, Lyu H Q, Yu A Z, Wang F, Li Y, Wang P F, et al. No-tillage mulch with green manure retention improves maize yield by increasing the net photosynthetic rate. European Journal of Agronomy, 2024; 159: 127275.

[6] Chen X Y, Jiang Z H, Yang J H, Ren J W, Rao Y, Zhang W. Data-driven decision support scheme for multi-area light environment control in greenhouse. Computers and Electronics in Agriculture, 2023; 211: 108033.

[7] Xu H Y, Huang C L, Jiang X, Zhu J, Gao X Y, Yu C. Impact of cold stress on leaf structure, photosynthesis, and metabolites in *Camellia weiningensis* and *C. oleifera* seedlings. Horticulturae, 2022; 8(6): 494.

[8] Moore C E, Meacham-Hensold K, Lemonnier P, Slattery R A, Benjamin C, Bernacchi C J, et al. The effect of increasing temperature on crop photosynthesis: from enzymes to ecosystems. Journal of Experimental Botany, 2021; 72(8): 2822–2844.

[9] Li Y F, Hou J Y, Yang Y X, Sun Z T, Gao P, Hu J. Multi-objective optimization of the light environment regulation model for greenhouse cucumber using mopso and topsis. Transactions of the Chinese Society of Agricultural Engineering, 2023; 39(19): 185–194. (in Chinese)

[10] Széles A, Huzsvai L, Mohammed S, Nyéki A, Zagyi P, Horváth É, et al. Precision agricultural technology for advanced monitoring of maize yield under different fertilization and irrigation regimes: A case study in eastern Hungary (Debrecen). Journal of Agriculture and Food Research, 2024; 15: 100967.

[11] Lin Y, Chen Z, Yu G R, Yang M, Hao T X, Zhu X J, et al. Spatial patterns of light response parameters and their regulation on gross primary productivity in China. Agricultural and Forest Meteorology, 2024; 345: 109833.

[12] Cui X L, Hu T T, Lu J S, Chen S H, Zhao L, Li A Q, et al. Reduced irrigation combined with nitrification inhibitor enhances grain yield and water-nitrogen use efficiency of winter wheat by improving the physiological characteristics. Journal of Agriculture and Food Research, 2025; 23: 102212.

[13] de Souza R R, Toebe M, Mello A C, Bittencourt K C. Sample size and shapiro-wilk test: An analysis for soybean grain yield. European Journal of Agronomy, 2023; 142: 126666.

[14] Gao P, Li B, Bai J H, Lu M, Feng P, Wu H R, et al. Method for optimizing controlled conditions of plant growth using U-chord curvature. Computers and Electronics in Agriculture, 2021; 185: 106141.

[15] Hou J Y, Li Y F, Sun Z T, Wang H Y, Lu M, Hu J, et al. A cooperative regulation method for greenhouse soil moisture and light using Gaussian curvature and machine learning algorithms. Computers and Electronics in Agriculture, 2023; 215: 108452.

[16] Zhao Y, Jie Z, Zhang Y, Jiang C, Cao Y H. Negative Gaussian curvature regulated pattern evolution on curved bilayer system. International Journal of Mechanical Sciences, 2024; 267: 108969.

[17] Pena J C, Napoles G, Salgueiro Y. Normalization method for quantitative and qualitative attributes in multiple attribute decision-making problems. Expert Systems with Applications, 2022; 198: 116821.

[18] Song P, Yue X, Gu Y, Yang T. Assessment of maize seed vigor under saline-alkali and drought stress based on low field nuclear magnetic resonance. Biosystems Engineering, 2022; 220: 135–145.

[19] Xian H F, Che J X. Unified whale optimization algorithm based multi-

kernel svr ensemble learning for wind speed forecasting. Applied Soft Computing, 2022; 130: 109690.

[20] Vanli N D, Sayin M O, Mohaghegh M N, Ozkan H, Kozat S S. Nonlinear regression via incremental decision trees. Pattern Recognition, 2019; 86: 1–13.

[21] Chen D Y, Zhang J H, Sun Z T, Zhang Z X, Hu J. Multi-objective optimal regulation model and system based on whole plant photosynthesis and light use efficiency of lettuce. Computers and Electronics in Agriculture, 2023; 206: 107617.

[22] Niu Y Y, Han Y X, Li Y D, Zhang M, Li H. Low-carbon regulation method for greenhouse light environment based on multi-objective optimization. Expert Systems with Applications, 2024; 252: 124228.

[23] Yang L, Song W W, Xu C L, Sapey E, Jiang D, Wu C X. Effects of high night temperature on soybean yield and compositions. Frontiers in Plant Science, 2023; 14: 1065604.

[24] Xu L H, Liu H, Wei R H. Research on integrated control strategy of light and CO_2 in blueberry greenhouse based on maximizing Gaussian curvature. Transactions of the Chinese Society for Agricultural Machinery, 2022; 53(7): 354–362. (in Chinese)

[25] Djuren T, Kohlbrenner M, Alexa M. K-surfaces: Bezier-splines interpolating at Gaussian curvature extrema. ACM Transactions on Graphics, 2023; 42(6): 210.

[26] Meyer M, Desbrun M, Schröder P, Barr A H. Discrete differential-geometry operators for triangulated 2-manifolds. In: Hege H C, Polthier K. (Ed.) Berlin, Heidelberg: Springer. Visualization and Mathematics III, 2003; pp.35–57.

[27] Hao S X, Cao H X, Wang H B, Pan X Y. The physiological responses of tomato to water stress and re-water in different growth periods. Scientia Horticulturae, 2019; 249: 143–154.

[28] Zhang J, Fang W K, Xu C D, Xiong A S, Zhang M C, Goebel R. Current optical sensing applications in seeds vigor determination. Agronomy-Basel, 2023; 13(4): 1167.

[29] Lu M, Liu H L, Xu J H, Li H M, Gao P, Mao H P, et al. A hybrid approach using chained-svr, mode and dea to optimize environmental control values in plant factories. Computers and Electronics in Agriculture, 2025; 233: 110211.

[30] Guerra M, Gomez R M, Sanz M A, Rodriguez-Gonzalez A, Casquero P A. Effect of fruit weight and fruit locule number in bell pepper on industrial waste and quality of roasted pepper. Horticulturae, 2022; 8(5): 455.

[31] Bedirhanoğlu V, Yang H, Shukla M K. Reducing water salinity at flowering stage decreases days to flowering and promotes plant growth and yield in chile pepper. Hortscience, 2022; 57(9): 1128–1134.

[32] Both A J, Benjamin L, Franklin J, Holroyd G, Incoll L D, Lefsrud M G. Guidelines for measuring and reporting environmental parameters for experiments in greenhouses. Plant Methods, 2015; 11: 43.

[33] Wen Y, Zhang Y Q, Cheng R F, Li T. Photosynthetic induction of the leaves varies among pepper cultivars due to stomatal oscillation. Scientia Horticulturae, 2023; 318: 112126.

[34] Li H M, Lu M, Yuan K K, Zhang M K, Wang D, Hu J. Acquisition and analysis of the optimal nutrient solution temperature range for lettuce using U-chord curvature. Int J Agric & Biol Eng, 2024; 17(6): 93–100.

[35] Yin J, Liu X Y, Miao Y L, Gao Y, Qiu R C, Zhang M. Measurement and prediction of tomato canopy apparent. Int J Agric & Biol Eng, 2019; 12(5): 156–161.

[36] Takagi D, Takumi S, Hashiguchi M, Sejima T, Miyake C. Superoxide and singlet oxygen produced within the thylakoid membranes both cause photosystem i photoinhibition. Plant Physiology, 2016; 171(3): 1626–1634.

[37] Wang K X, Xing Q F, Ahammed G J, Zhou J. Functions and prospects of melatonin in plant growth, yield, and quality. Journal of Experimental Botany, 2022; 73(13): 5928–5946.

[38] Queensland government, drought and climate adaptation program. Capsicum - critical temperature thresholds. 2020. Available: https://data.longpaddock.qld.gov.au/static/dcap/DCAP3/DCAP%203__3%20Capsicum%20CTT%20Final.pdf. Accessed on [2020-12-09].